Earth, Planets and Space

FULL PAPER

Open Access

ZWDX: a global zenith wet delay forecasting model using XGBoost

Laura Crocetti[1*] , Matthias Schartner[1] , Marcus Franz Wareyka-Glaner[2] , Konrad Schindler[1] and Benedikt Soja[1]

Abstract

Tropospheric delays play a crucial role for Global Navigation Satellite Systems (GNSS). They are a major error source in GNSS positioning and, at the same time, also a variable of interest in GNSS meteorology. Regardless of whether the delay shall be eliminated or inverted to atmospheric parameters, and no matter how this is done, it is of utmost importance to accurately determine tropospheric delays. In this study, we present a global zenith wet delay (ZWD) model, called ZWDX, that offers accurate spatial and temporal ZWD predictions at any desired location on Earth. ZWDX is based on the XGBoost algorithm and uses ZWDs measured at over 19,000 GNSS stations as reference. The inputs of ZWDX are the geographical location, observation time, and specific humidity at nine atmospheric pressure levels. For our study, we train the model on the years 2010 to 2021 and then test it for the year 2022. While ZWDX is trained to predict ZWD values based on specific humidity values from the ERA5 reanalysis, we show that it also delivers good predictions when applied to HRES specific humidity forecasts, making it suitable for (short-term) ZWD forecasting. The ZWDX model predictions are evaluated at 2500 globally distributed, spatio-temporally independent GNSS stations, with forecasting horizons ranging from 0 h to 48 h, and achieve root mean squared errors (RMSE) between 10.1 mm and 16.2 mm. To independently evaluate ZWDX's performance and to demonstrate its potential for a real-world downstream task, we use its predictions as a-priori values for a precise point positioning (PPP) analysis and compare the results with those obtained using ZWD values from VMF1 or VMF3. We find that the highest accuracy and fastest convergence are indeed achieved with ZWDX.

Keywords Zenith wet delay (ZWD), Global predictions, XGBoost, Machine learning (ML), GNSS, Precise point positioning (PPP)

*Correspondence:
Laura Crocetti
lcrocetti@ethz.ch
Full list of author information is available at the end of the article

Crocetti *et al. Earth, Planets and Space*   (2024) 76:163

Page 2 of 16

Graphical Abstract

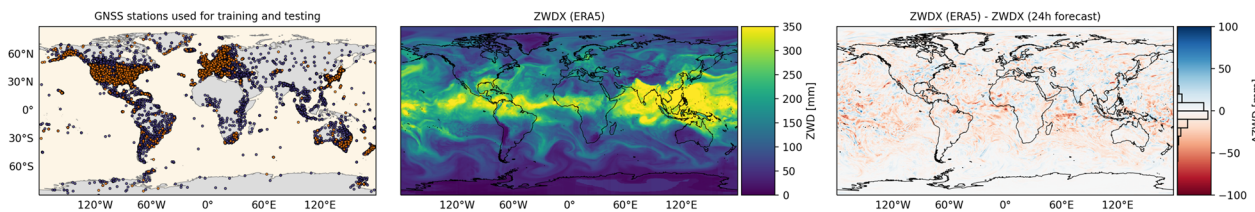## ZWDX: A Global ZWD Forecasting Model Using XGBoost

Input:
- Geographical location
- Observation time
- Specific humidity

Output:
- Accurate ZWD forecasts at any desired location on Earth

Evaluation:
- Performance on unseen data
- Comparison with VMF1 and VMF3
- GNSS Precise Point Positioning

1 Introduction

Global Navigation Satellite Systems (GNSS) are primarily known for positioning and navigation applications, but they also play an important role in gathering meteorological information. Their emitted signals traverse the atmosphere, where they are delayed. The delay depends on the properties of the atmosphere and the signal path, e.g. its constituents and their densities. By precisely measuring these delays, one can derive insights into the current state of the troposphere (the lowest part of the atmosphere), an indirect observation technique referred to as "GNSS meteorology" (Bevis et al. 1992). GNSS meteorology makes use of ground-based GNSS receivers, and optionally also of GNSS measurements received at low-Earth orbiting satellites, via the radio occultation (RO) technique (Ware et al. 1996). Of particular interest in this context is the amount, distribution, and change of tropospheric water vapour, a core variable for weather forecasting and climate modeling.

During the analysis of GNSS signals, the tropospheric delay is divided into a hydrostatic component and a wet component. Both components are parameterized by specifying the delays along the zenith direction, which can be mapped to other ray directions with the help of the associated elevation angle (Böhm 2013). Consequently, the quantities needed to characterize the influence of the troposphere on the signal runtime are the *zenith hydrostatic delay* (ZHD) and *zenith wet delay* (ZWD), which together make up the *zenith total delay* (ZTD). While the hydrostatic part can be modeled with sufficient accuracy, the wet part is less predictable and has to be estimated during GNSS analysis.

The wet delay is particularly important for GNSS meteorology, as it is proportional to the atmospheric water vapour content along the signal path. ZWD can be transformed into the mass of *integrated water vapour* (IWV) in a vertical atmospheric column over a unit area and into *precipitable water vapour* (PWV), the height of an equivalent column of liquid water. RO, in contrast, provides vertical profiles of atmospheric refractivity, which in turn enable the estimation of water vapour concentration. All of these GNSS-derived tropospheric data products contribute to a better understanding of various meteorological phenomena.

The paper by Bonafoni et al. (2019) reviews the use of RO and ground-based GNSS products in the context of extreme weather events. They found that ground-based GNSS products are most frequently used to analyse convective storms and heavy rainfall events, while RO products are mostly used to investigate tropical cyclones. A study by Aichinger-Rosenberger et al. (2022) used GNSS troposphere products to detect and predict foehn winds at the meteorological observation site in Altdorf, Switzerland. Li et al. (2021a) used GNSS troposphere measurements to detect heavy precipitation events in Hong Kong. GNSS-derived PWV and meteorological parameters were used by Liu et al. (2022) to develop a rainfall forecasting model for Singapore, and by Benevides et al. (2019) to make short-term forecasts of intense rainfall in the Lisbon area in Portugal. Another study by Ziv and Reuveni (2022) has demonstrated the potential of predicting flash floods over the eastern Mediterranean from PWV estimates derived from GNSS tropospheric delays. Łoś et al. (2020) have developed a GNSS-based storm nowcasting method that combines IWV with vertical

Crocetti *et al. Earth, Planets and Space* (2024) 76:163

Page 3 of 16

profiles of wet refractivity from GNSS tomography, while Guerova et al. (2022) have demonstrated storm nowcasting based on troposphere data products.

These studies show the potential of GNSS-based troposphere monitoring for diverse meteorological phenomena. Still, dense spatio-temporal modeling and forecasting of ZWD, the basis for all products, remains challenging and is not done consistently. Instead, several ZWD models exist. Among the most popular are the discrete Vienna mapping function 1 (VMF1; Böhm et al. 2006, 2009), its successor VMF3, and the empirical global pressure and temperature 3 model (GPT3; Böhm et al. 2015; Landskron and Böhm 2018a, b).

Improving troposphere models and addressing the deficits of existing models is an active area of research. For instance, GPT3 is known to have lower accuracy than the VMFs and is only available on coarse 5 × 5 degree and 1 × 1 degree grids. On the other hand, it was found that the VMF1 has location-dependent systematic errors because it has been tuned for specific elevation angles, station heights, and orbital altitudes (Zus et al. 2015).

In recent years, a number of studies have explored the possibility of enhancing troposphere models with the help of various machine learning (ML) techniques (Siemuri et al. 2022). Lu et al. (2023) have developed a tropospheric delay forecasting model for the contiguous USA based on a convolutional long short-term memory (LSTM) network. Their model, called TropNet, is trained on ZWDs derived at 165 GNSS stations between April 1 and July 31, 2019, and then tested at 20 different GNSS stations for the same period. As input features it uses water vapour channel radiances, tropospheric delays, and topography data. TropNet forecasts ZWDs with a lead time up to 6 h and at a spatial resolution of 2 km, and achieves a root mean squared error (RMSE) around 1.15 cm compared to GNSS-derived reference ZWDs. He et al. (2024) also use an LSTM to create a global tropospheric forecasting model, trained on ZTD residuals on a global 5 × 5 degree grid (after removing the periodic signal component). The years from 2008 to 2019 serve as training period, and the year 2020 was used for testing. The combined model, including both the periodic component and the predicted deviations from it, delivers ZTDs with an average RMSE of 1.44 cm. Another recent study by Li et al. (2024) combines a neural network and a Random Forest to model ZWD. The model is trained on reference ZWDs derived from radiosonde observations at 569 sites from 2015 to 2019 and GPS RO profiles from 2016 to 2019. In their experiments the model, which, besides the location and day of year, also includes meteorological predictors like surface water vapour pressure and surface temperature, improved the ZWD forecasting accuracy by up to 23.8 %. In a comparison at 609 sites,

the model predictions deviate 3.1 cm from radiosonde observations, respectively 2.4 cm from RO data.

All these models demonstrate improvements over classical models with the help of data-driven ML, on the other hand they still have deficits. First, many have been derived based on only a small number of stations and/or limited time periods. Thus, they are likely to generalize poorly beyond the limited atmospheric conditions represented in their training data. Some models are explicitly designed to be applicable only in a specific region (Li et al. 2021b, 2023; Yang et al. 2021). Others do not specify the application domain, but have been tested only within the same year or in a different year but at the same stations, not with spatio-temporally independent samples (Chen and Gao 2024; Lu et al. 2023; Selbesoglu 2020). Furthermore, most models are not designed for forecasting, since they require inputs for which no operational forecasts are available (Li et al. 2024; Bi et al. 2024; Xia et al. 2020). Finally, none of the described models is—to the best of our knowledge—openly accessible and deployable.

Our study aims to address these limitations by introducing ZWDX, a broadly applicable, global ZWD model. ZWDX represents a major improvement over our previous study, in which we already introduced a ZWD model able to derive global, spatially explicit ZWD fields with an accuracy below 1 cm (Crocetti et al. 2024b). That model was also based on the XGBoost algorithm, a versatile ensemble estimator popular across a wide range of scientific prediction tasks. It employed observations from over 13,000 globally distributed GNSS stations, together with meteorological predictors, to obtain high-accuracy ZWD estimates anywhere on Earth. However, the focus of the model was on the *spatial ZWD distribution*, whereas it did not aim for temporal generalisation outside the reference period of 1 year, thus ignoring inter-annual variability. In fact, that model was by design not suitable for forecasting (or nowcasting), given that its inputs were extracted from the ERA5 reanalysis (Hersbach et al. 2020), which has a latency of five days.

In the present study, we address these limitations and extend our model to additionally predict future ZWD values at arbitrary locations, based only on inputs that are available in real-time. The new model, called ZWDX, is again based on the XGBoost algorithm. It has been trained with ERA5 data covering a period of 12 complete years (2010–2021) and 16,664 GNSS stations, so as to cover to the largest possible extent the spatio-temporal variability of the atmospheric conditions that determine the ZWD.

To summarize, the goal of the present study is to develop and validate a data-driven ZWD model that offers high-quality predictions at any desired location on
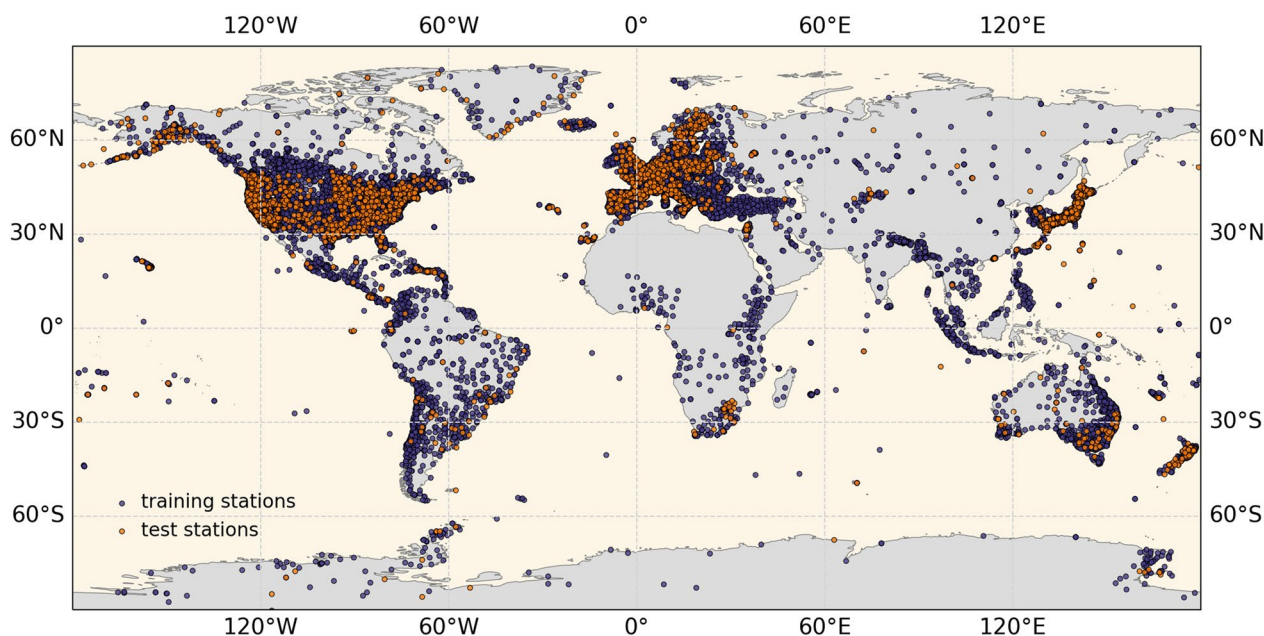
Fig. 1 Distribution of the 19,260 GNSS stations, divided into training (blue) and test (orange) stations

Earth, and for any point in time (within the period for which state-of-the-art atmospheric reanalysis data are available). ZWDX is designed to be versatile and cater to various applications that require ZWD estimates. For GNSS meteorology, the model delivers ZWD estimates not only at GNSS station locations but also densely across geographic regions of arbitrary extent, enabling comprehensive spatial analysis in regions that lack a high-density GNSS station network. Furthermore, the possibility to drive the model with HRES forecasts (as opposed to post-processed ERA5 data) opens up the possibility to forecast future ZWD values without temporal lags. ZWDX has already demonstrated potential for climate studies (Crocetti et al. 2024a). Finally, ZWDX can be used to obtain a-priori values needed for space-geodetic parameter estimation, including high-end GNSS processing and Very Long Baseline Interferometry (VLBI). Here, we validate the potential of ZWDX for such downstream by using its predictions to initialise precise point positioning (PPP). In that experiment (Sect. 4.2), ZWD values estimated with ZWDX match or even slightly surpass those from state-of-the-art models like VMF3, furnishing independent evidence for our model's reliability.

Section 2 introduces the data used in the present study including the ZWD reference (Sect. 2.1), specific humidity (Sect. 2.2) and VMFs (Sect. 2.3). Section 3 describes the setup of the ZWDX model, its parameters, and the

performance metrics used to evaluate it. Furthermore, we also describe how PPP is employed to investigate the impact of ZWDX on a real-world GNSS application. Experimental results are shown and discussed in Sect. 4 before Sect. 5 offers our conclusions from the study and a brief outlook.

2 Data

2.1 Zenith wet delay (ZWD)

Our study utilizes ZWD values at 19,260 globally distributed GNSS stations from 2010 to 2022. They are provided by the Nevada Geodetic Laboratory (NGL; Blewitt et al. 2018) using the GipsyX version 1.0 software[1] (Bertiger et al. 2020). A substantial advantage of this data set lies in its global coverage and considerable volume, required to derive a robust, globally applicable ZWD model; and in the fact that it has been processed uniformly by a single analysis center, which ensures consistency.

The temporal resolution of the original NGL ZWD data is five minutes. As a first step, the data is down-sampled to match the hourly resolution of the meteorological variables discussed in Sect. 2.2, by calculating a weighted mean of the ZWDs in a 60-minute window centered on each full hour. The weight is highest for the value at the full hour and decreases linearly towards the limits of the 60-minute interval.

Of the 19,260 GNSS stations, 16,760 were selected as training stations, while the remaining 2500 serve as test stations. The test stations were chosen randomly among those stations that cover the entire period from 2010

---

[1] A comprehensive description of the underlying methodology can be found at http://geodesy.unr.edu/gps/ngl.acn.txt; last access: 10.11.2024.

Crocetti *et al. Earth, Planets and Space*   (2024) 76:163

Page 5 of 16

to 2022. In total this amounts to $\approx$ 841 million (potential) training samples and $\approx$ 247 million test samples for model evaluation, corresponding to a 77/23 % split.

The geographic distribution of the training and test stations is depicted in Fig. 1. While most GNSS stations are located in the Northern Hemisphere, mainly in the United States, Europe, and Japan, the density of GNSS stations is noticeably lower in the Southern Hemisphere, particularly in Africa.

The quality of the NGL tropospheric products has been analyzed in several studies, by comparing it to tropospheric delays derived with the GPT3 model or with ray-tracing (Ding and Chen 2020; Ding et al. 2023), as well as by transforming NGL ZWD values to IWV or PWV and comparing them to radiosonde observations (Yuan et al. 2023; Ding et al. 2022). Despite the generally satisfactory quality, a rigorous outlier screening was carried out for the training data to ensure that only plausible ZWD data are used for model fitting: (i) based on the standard deviations reported as part of the product, the 1 % ZWDs with the highest uncertainties were removed. The threshold of 1 % was selected empirically based on the distribution of the reported standard deviations, with the aim of eliminating obvious outliers. (ii) negative ZWD values that lack physical meaning were eliminated. These values likely stem from automatic procedures trying to compensate erroneous ZHD estimates. (iii) ZWDs deviating from the 5-hour floating median by more than $3 \times$ their standard deviation were filtered out to further remove large outliers. (iv) locations with two or more co-located stations within a distance of 1 km were inter-compared. 1424 such co-located station groups with, in total, 3234 stations were identified. For each group the median ZWD was calculated per epoch, and stations with a bias above 5 mm w.r.t. that median value (59 out of the 3234 candidate stations) were removed.

Taken together, the four filtering steps discarded 2.5 % of the ZWD training data (21,146,511 samples), resulting in a final training data set of 820,548,217 samples distributed over 16,664 GNSS stations. The independent test set was not filtered at all, so as to ensure a realistic and fair evaluation.

2.2 Specific humidity

Our ZWDX model utilizes specific humidities provided by the European Centre for Medium-Range Weather Forecasts (ECMWF). The centre offers different types of data:

(i) Its Reanalysis v5 (ERA5) data set (Hersbach et al. 2020) is available on a regular latitude-longitude grid with a spatial resolution of 0.25 degrees. It has a 1-hour temporal resolution and includes 37 pressure levels ranging from 1000 hPa to 1 hPa. ERA5 is

a reanalysis that is made available with a latency of 5 days. Consequently, it cannot directly be used for ZWD forecasting. ERA5 is considered to be one of the best data sets of atmospheric variables, as confirmed by several studies. Recently, it has been used as reference data to train AI-based global weather models that, for the first time, outperformed traditional forecasting models, including GraphCast (Lam et al. 2023) and Pangu-Weather (Bi et al. 2023). It is thus a natural basis for our data-driven ZWDX model.

(ii) Forecasts from ECMWF's highest-resolution forecasting model (HRES). HRES provides four runs per day (at 00/06/12/18 UTC) and is therefore suitable for real-time applications. Each run offers hourly forecasts of the meteorological variables, including specific humidity, up to a horizon of 90 h on a 0.25-degree latitude-longitude grid. These forecasts are available for 25 pressure levels that overlap the 37 levels of the reanalysis. HRES is considered to be among the best global medium-range weather forecasts and is used for instance in WeatherBench 2 (Rasp et al. 2024) as a benchmark for data-driven global weather prediction models. Again, it constitutes a natural data source for ZWDX.

Out of the available pressure levels, we select nine as input for ZWDX (1000, 950, 925, 900, 850, 800, 700, 600, 500 [hPa]), based on experience from our earlier study (Crocetti et al. 2024b). All these levels are available in both ERA5 and HRES. While specific humidity values from the ERA5 are used to train ZWDX, specific humidity forecasts from HRES are used as input at test time to predict future ZWD values. Despite their high quality, both data sets contain uncertainties and errors. These uncertainties are not considered in the training process of ZWDX. Users should be aware that these propagate and may degrade the predictions of ZWDX (or of any other model that uses them). Explicit modeling of input uncertainties may be an interesting direction for future work.

2.3 Vienna mapping functions (VMFs)

As an independent evaluation of the proposed ZWDX model, we compare ZWDX to the ZWD products from VMF1 and VMF3, for the application of PPP, see Sect. 3.2. All VMF products are provided via the VMF data server.[2] There are operational versions, published at ca. 18:00 UT for the previous day; and forecast versions, published ahead of time at ca. 09:00 UT for the following

---

[2] https://vmf.geo.tuwien.ac.at/; last access: 10.11.2024.

Crocetti *et al. Earth, Planets and Space*   (2024) 76:163

Page 6 of 16

day. VMF3 forecasts have 1×1 degree resolution, while VMF1 forecasts have 2×2.5 degree resolution. Moreover, VMF parameters are provided on a regular, global grid and as site-wise products for designated stations. For a meaningful comparison to ZWDX, we use the gridded forecast versions of VMF.

3 Methodology

3.1 ZWDX model setup

Our ZWDX model is trained on 12 years of data and based on Extreme Gradient Boosting (XGBoost; Chen and Guestrin 2016). XGBoost is an efficient, scalable ML algorithm based on an ensemble of regression trees, which are iteratively fitted with gradient boosting. The choice of algorithm is based on extensive empirical investigations carried out in Crocetti et al. (2024b). In that previous study, the model already proved to be very robust, thanks to the large sample size and to the regularization techniques applied during XGBoost training. ZWDX can be expected to have even greater robustness, given that its training set is an order of magnitude larger.

The target variables are station-wise ZWD values. The period comprising 2010 to 2021 is used to train the XGBoost model, while the year 2022 serves as test set for evaluation. The input features are: GNSS station coordinates (latitude ϕ, longitude λ, height h), relative time information (day of year *doy*, hour of day *hod*), and specific humidity q at nine pressure levels. Specific humidity values at the precise GNSS station location are derived through bilinear interpolation in the $0.25°$ grid. To account for the cyclic nature of *doy*, *hod*, and λ, they are transformed to pairs of $\sin(\cdot)$ and $\cos(\cdot)$ values, resulting in two features per variable. Overall, the feature vector for a given location and time has 17 dimensions, which are all standardized prior to feeding them into the XGBoost model.

The hyper-parameters of the XGBoost algorithm were tuned for optimal performance through a grid search with 6-fold cross-validation. As that procedure is computationally expensive, it was run using only data samples from 1 year (2019). Going beyond our earlier work, we made sure it was ensured that individual folds are independent in space *and* time. To that end, we held out a fixed set comprising 20 % of the training stations as validation set. Then, the data was temporally partitioned into six folds, each consisting of two consecutive months. During hyper-parameter tuning, the model was trained on five temporal folds of the training stations and evaluated on the sixth temporal fold at the validation stations. That is, the test data was from locations and epochs that were never seen by the model during training, so as to maximize its capability to generalize across space and time. The procedure was repeated six times, such that

each temporal fold was once used for validation. The average performance over the six runs was then compared to select the most appropriate XGBoost settings, which turned out to be 200 trees, each with a maximum tree depth of 10, and a learning rate per boosting iteration of 0.05. With those hyper-parameters the ZWDX model was retrained using the full set of training stations (including the validation stations) and the entire time period from 2010 to 2021.

The resulting model was then evaluated on the independent test stations for the year 2022, which again have no spatial or temporal overlap with the training set. The predicted ZWDs for the test stations $\hat{y}_i$ are compared to the reference ZWDs of NGL, y_i. We compute the station-wise RMSE values (Eq. 1) for all test stations and combine them into a final, global performance metric by taking the weighted mean (WRMSE; Eq. 2) with weights proportional to the number of samples at a station (#samples$_i$):

$$\text{RMSE}_i = \sqrt{\frac{\sum_j^{\#\text{samples}_i}(y_{i,j} - \hat{y}_{i,j})^2}{\#\text{samples}_i}} \qquad (1)$$

$$\text{WRMSE} = \frac{\sum_i^{\#\text{stations}}\left(\#\text{samples}_i \cdot \text{RMSE}_i\right)}{\sum_i^{\#\text{stations}}\left(\#\text{samples}_i\right)} \qquad (2)$$

The ZWDX model was trained on the specific humidity of the ERA5 reanalysis data set. However, since ERA5 cannot be directly used for forecasting into the future due to its delayed availability, we also tested the performance of our ZWDX model (still trained on ERA5) when feeding it with HRES forecast data instead. Thus, the evaluation of ZWDX is run twice, once with the ERA5 observations at the test stations to isolate the predictive skill of the model from the quality of its inputs, and once with the HRES forecast data at the test stations to evaluate the true forecasting performance one can expect in an operational real-time setting, including errors due to inaccuracies of the HRES forecast values of specific humidity. Different forecasting (respectively, nowcasting) horizons from 0 to 48 h were examined, abbreviated as F*xx* (e.g., F24 corresponds to the 24-hour forecasts).

3.2 Evaluation of ZWDX with PPP

Besides comparing the ZWDX predictions directly to the reference values from NGL, we further indirectly evaluate their impact on a standard downstream task, namely precise point positioning (PPP). PPP requires a-priori ZWD values to initialise the computation. The aim of the experiment is to verify that ZWDX predictions are reliable and suitable as input for the downstream task. That is, we check whether PPP based on ZWDX reaches accuracies and convergence times comparable to those

Crocetti *et al. Earth, Planets and Space*   (2024) 76:163

Page 7 of 16

Table 1 Processing settings of raPPPid

Software	raPPPid (VieVS PPP)
Stations	25 globally distributed IGS MGEX stations (Fig. 10 in the appendix)
Period	Year 2022
Processing mode	Static, post-processing, ionosphere-free linear combination
Observations	GPS L1 and L2, Galileo E1 and E5a
Observation interval	30 s, reset of the solution every 45 min
Observation ranking	GPS: WC, Galileo: CQX
Raw observation noise	Code 30 cm, phase 2 mm
Observation weighting	Elevation based weighting, $\sin(elev^2)$, cutoff angle: 5°
Satellite products	MGEX orbits, clocks, and biases from Center of Orbit Determination Europe (CODE)
Troposphere model	ZWDX **or** VMF3 (forecast, 1 × 1 degree, gridwise) **or** VMF1 (forecast, 2 × 2.5 degree, gridwise)
Correction models	Relativistic effects, Phase Wind-Up, receiver antenna height, phase center offsets and variations, solid Earth tides, ocean loading, pole tides, Shapiro effect
Adjustment	Extended Kalman Filter (float solution) and Least-Squares-Adjustment (fixed solution)
Parameters	Receiver coordinates, GPS receiver clock error, Galileo receiver clock offsets, float ambiguities
Cycle-slip detection	$dL_i - dL_j$ (threshold = 0.05 m)
Outlier detection	Check of observed minus computed (code threshold = 25 m, phase threshold = 2 m)
PPP-AR	Fixing cutoff: 10°, fixing starts after 120 s, the highest satellite is selected as reference satellite

with other state-of-the-art ZWD models. If they do, this would provide further, independent evidence for the reliability of our model. We do not expect large gains in accuracy, given that PPP refines the ZWD values as part of its processing and therefore may converge to the same optimum from different a-priori values. While faster convergence may indicate a-priori values closer to the final optimum, but the speed-up (if any) also depend on the detailed behaviour of the underlying numerical optimisation scheme. Perhaps most importantly, the experiment highlights that ZWDX performs at least on par with some of the best current ZWD models and represents a viable alternative.

PPP is a standard GNSS processing technique used in various applications (Kouba et al. 2017; Geng 2022), where the absolute position of a GNSS receiver is determined with the help of precise satellite products and observation models (Glaner 2022). PPP offers several advantages over relative positioning methods and nowadays can achieve centimeter-level positioning accuracy, similar to that of the widely used relative Real-Time-Kinematic (RTK) mode. The primary concern with PPP is the rather long convergence time needed until the estimated parameters have reached the desired accuracy.

We carry out PPP analysis with the open-source software raPPPid (Glaner and Weber 2023), based on dual-frequency GPS and Galileo observations at 25 globally distributed stations in the International GNSS Service (IGS; Johnston et al. 2017) Multi-GNSS Experiment

(MGEX) for the year 2022 (Fig. 10 in the appendix). Table 1 summarizes the settings of the PPP processing. For a detailed explanation of the settings please refer to the raPPPid wiki[3] and Glaner (2022).

The GNSS observations are processed using the ionosphere-free linear combination. Float and fixed coordinate solutions are computed, estimating the phase ambiguities as real values or integer values, respectively. The float solution is calculated with an Extended Kalman Filter, while Least Squares Adjustment is used for the fixed solution (Glaner 2022). The fixing process is started after two minutes, since several epochs with valid float solutions are required to correctly fix the integer ambiguities. To model the tropospheric delays, ZWDX estimates are introduced in the PPP observation model together with the corresponding ZHD values taken from the VMF3. As a benchmark, we perform two more PPP runs, where we use VMF1 or VMF3, respectively, for the tropospheric delays instead of ZWDX.

The PPP processing was restarted every 45 min. After every restart, we measure the convergence time and positioning accuracy with all three troposphere models. Overall, this procedure yields ≈ "272, 000" convergence periods for 25 stations and one full year of data (slightly less than the theoretically achievable 292,000 45 min intervals, due to occasional periods of missing data). Convergence is defined as the time when the 2D coordinate difference has fallen below 10 cm for the float solution or below 5 cm for the fixed solution and remains below that threshold for the remainder of the 45 min interval (Glaner 2022).
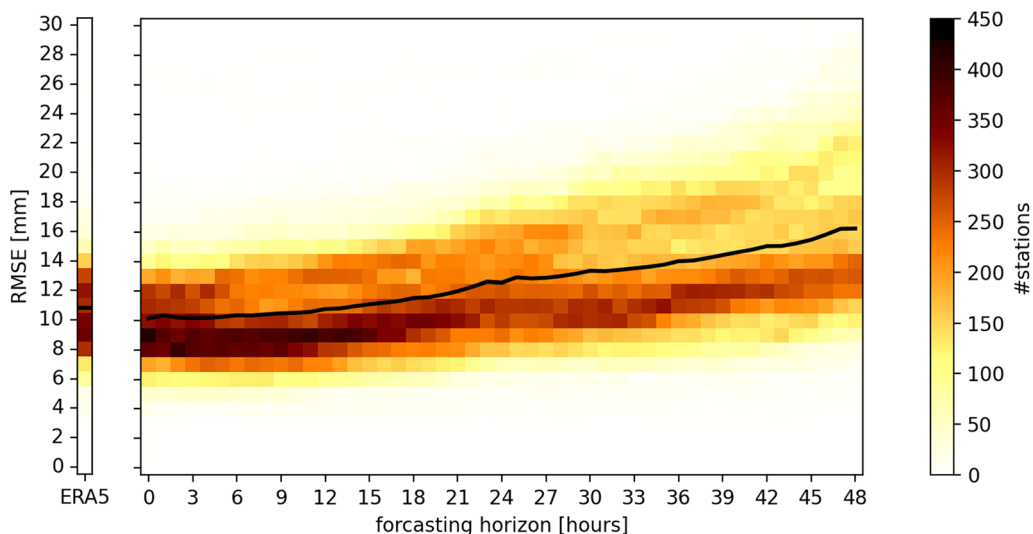

Fig. 2 RMSE over 2500 test stations that are both spatially and temporally disjoint from the training set, using as input either ERA5 (left) or HRES (right) with forecasting horizons between 0 to 48 h (F00–F48). Colors denote the number of stations, the black line denotes the WRMSE
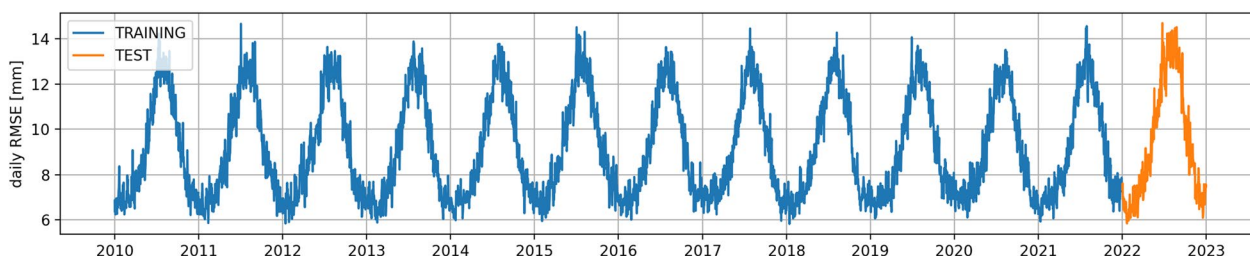

Fig. 3 Daily RMSE over the test stations for the training (blue) and testing (orange) periods, using ERA5 as input

The ZWD is normally estimated as part of the PPP solution to account for small-scale and unpredictable variations, e.g., due to the local weather. Here, we instead plug in the ZWD values predicted by a troposphere model (ZWDX, VMF1, or VMF3), such that imperfections of that model manifest themselves as range errors and propagate to float coordinates (and associated ambiguities); which then, in turn, degrade integer ambiguity fixing. In this way, one can assess the impact of different troposphere models on the quality of GNSS positioning.

4 Results

4.1 Performance of ZWDX

To assess the performance of our model on unseen data, it is applied to data recorded in the year 2022 at 2500 held-out GNSS stations. That is, the test data are from locations and from a time interval never seen during training. We run ZWDX twice for those stations, once with specific humidities from the ERA5 reanalysis (as used during training), and once with HRES forecast data at various horizons (as in a real-time, forecasting setting).

The predictions are then compared to GNSS ZWD estimates from NGL, which are viewed as the reference values.

The performance on the test stations for the year 2022, in terms of RMSE, is depicted in Fig. 2. With ERA5 specific humidity data, the deviations from the NGL reference lie between 6 and 15 mm (0.05 and 0.95 quantiles) with a WRMSE of 10.8 mm. With HRES specific humidity forecasts the performance obviously depends on the forecasting horizon. As expected, the WRMSE is lowest at F00 with 10.1 mm, and then slowly increases up to 16.2 mm at F48. We note that HRES forecasts are processed every 6 h with a latency of about 6 h, so forecasts beyond $\approx$ 12 h will normally not be required in practice. For these practically relevant horizons the ZWD accuracy remains below 10.8 mm.

To conclude, we find that feeding the ZWDX model HRES forecasts (with a reasonable horizon) instead of ERA5 data does not harm the quality of its ZWD predictions. Consequently, we conclude that the HRES forecasting accuracy is good enough for (short-term) ZWD
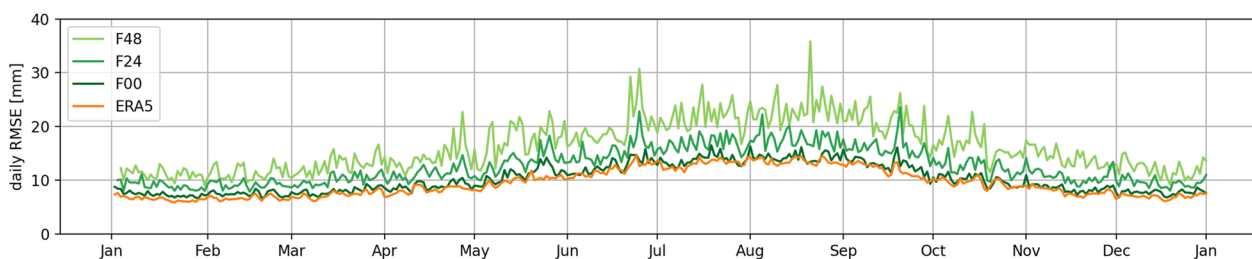
Fig. 4 Daily RMSE over the test stations for the test period, using either ERA5 (orange) or HRES (green) as input
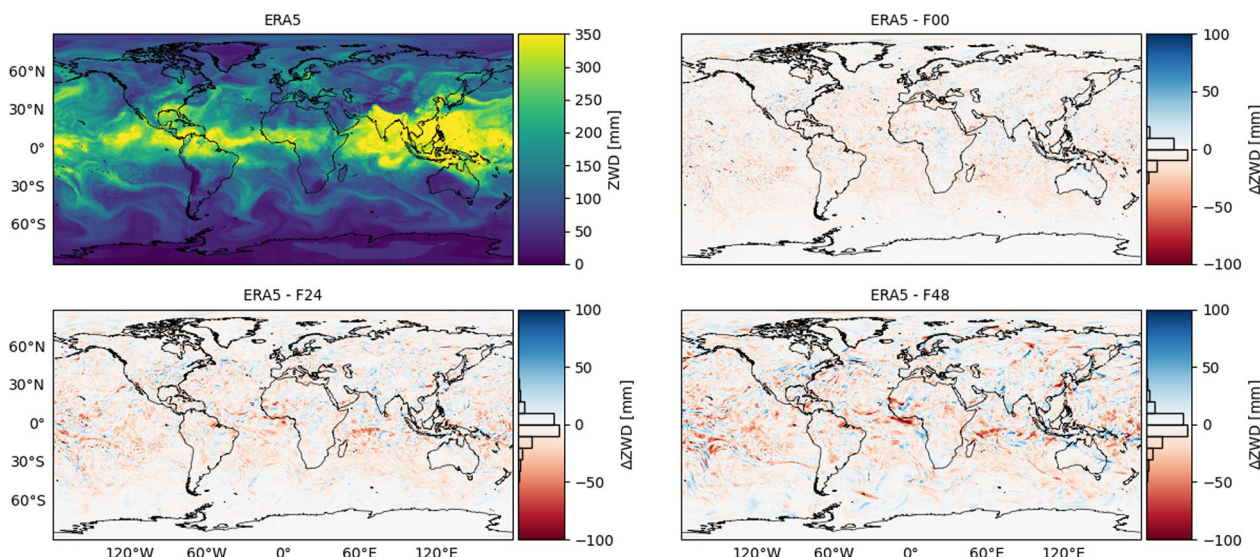

Fig. 5 Global ZWD predictions for July 1, 2022, 00:00 UTC based on ERA5 (top left), and differences to predictions based on HRES forecasts with horizons F00 (top right), F24 (bottom left), and F48 (bottom right). Histograms inside the colorbars depict the distribution of the deviations

forecasting. Somewhat counter-intuitively, the WRMSE with HRES forecasts up to a horizon of 12 h is slightly lower than with post-processed ERA5 data. For our purposes the tiny difference (below 0.7 mm) is irrelevant, still it may be interesting for future work to investigate what causes this effect.

To contrast the prediction performance for the training and test periods and to ensure no overfitting occurs, we calculated per-day RMSE values over the test stations for the entire time window 2010–2022, see Fig. 3. Overfitting happens when a model latches onto spurious patterns in the training data, and thus fails to make accurate predictions on new, unseen data. In previous works, we observed temporal overfitting, meaning that the model predictions had significantly higher errors for epochs outside the training period (Crocetti et al. 2024b). The similar performance of ZWDX for both the training and testing periods (see Fig. 3) confirms that the model does not overfit temporally and can reliably predict ZWD for new epochs, which is an important improvement. The

daily RMSE during the test period is only slightly worse (9.5 mm) than during the training period (9.1 mm); indicating that the ZWDX model generalizes well and can handle the atmospheric conditions encountered in 2022 based on those observed in the preceding 12 years. Furthermore, the error curves of different years are very similar, meaning that the model is able to absorb inter-annual variability due to multi-year atmospheric oscillations.

The daily RMSE time series highlights a prominent seasonal signal. This is consistent with the known seasonal variations of ZWD: Higher temperature and humidity during summer cause an increase in ZWD and the associated uncertainty, especially in tropical climates. The much larger number of stations in Europe, North America, and Japan means that the seasonal behavior of the Northern Hemisphere dominates.

To examine the impact of the forecasting uncertainty in more detail, we also calculate daily RMSEs for ZWD time series derived from HRES forecasts for the year 2022, with three different forecasting horizons [F00, F24, F48],
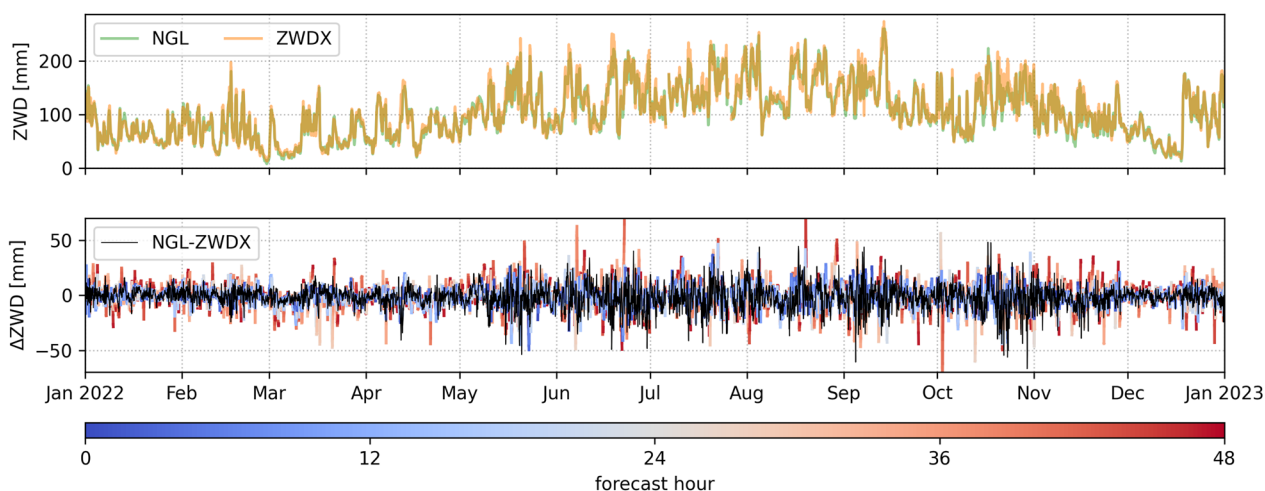
Fig. 6 Time series for GNSS station BRUX. Top: ZWD from NGL (green) and from ZWDX driven by ERA5 (orange). Bottom: Deviations between NGL and ZWDX driven by ERA5 (black), as well as between NGL and ZWDX driven by HRES (forecasting horizon color-coded from blue to red)

Table 2 WRMSEs [mm] of the test stations between different troposphere models

	NGL	ZWDX	VMF1
ZWDX	10.8		
VMF1	15.2	14.5	
VMF3	12.2	11.4	7.9

see Fig. 4. The corresponding average per-day RMSEs are [10.2, 12.6, 16.3] mm, respectively, again confirming the gradual inflation of the prediction errors as one increases the horizon. As a baseline, we also show the time series of daily RMSEs based on ERA5 specific humidities (cf. Fig. 3).

The ZWDX model can predict a ZWD value at any desired location on Earth and for any point in time for which ERA5/HRES fields are available. As an example, we have estimated ZWD values on a dense latitude/longitude grid with 0.25° grid spacing, for July 1, 2022, at 00:00 UTC, see Fig. 5. To study whether there are systematic patterns of deviation between predictions based on (presumably more accurate) ERA5 reanalysis data or in HRES forecasts with varying horizon, we compute four such maps using [ERA5, F00, F24, F48] and display pairwise differences between ZWDs based on ERA5 or on HRES forecasts. As suggested by the earlier quantitative comparisons, ERA5 and F00 are very similar: on average the ZWD values differ by 5.2 %. For longer horizons, they then slowly increase, to 6.4 % for F24 and 8.5 % for F48, respectively. Importantly, there are no discernible geographic patterns. The differences are centered around zero and distributed fairly uniformly across the Earth,

suggesting that using ZWDX with HRES forecast data (rather than data from ERA5 reanalysis) does not introduce regional biases.

Figure 6 compares the reference ZWD from NGL to ZWDX estimates, exemplary for the GNSS test station BRUX, located in Belgium. The top plot shows that the ZWDX estimates (orange) are in close agreement with the reference ZWDs from NGL (green), with a correlation of 0.98. In the bottom plot, we display the deviations between the reference and ZWDX predictions based either on ERA5 (black line) or on HRES (color-coded according to the forecasting horizon). The plot again confirms that the progressively larger uncertainty of longer-term forecasts does not lead to systematic biases. Rather, it causes zero-mean fluctuations with higher amplitude, particularly during the summer months, where ZWD values are generally larger due to the higher water vapour concentration.

Finally, an inter-comparison between NGL, ZWDX, and the VMFs is carried out. To that end, we compute ZWDs for the test stations with the different troposphere models and compare them in terms of WRMSE, see Table 2. ZWDX reproduces NGL ZWDs better (10.8 mm) than both VMF1 (15.2 mm) and VMF3 (12.2 mm). The comparison between ZWDX and the VMFs shows a better agreement for VMF3 (11.4 mm) than for VMF1 (14.5 mm). For the sake of completeness, we also compared VMF1 and VMF3, which agree well with a WRMSE of 7.9 mm.

4.2 Performance of PPP analysis
ZWDX is a generic, versatile ZWD model that can be employed in a range of applications. Here, we use PPP to

Crocetti *et al. Earth, Planets and Space*   (2024) 76:163
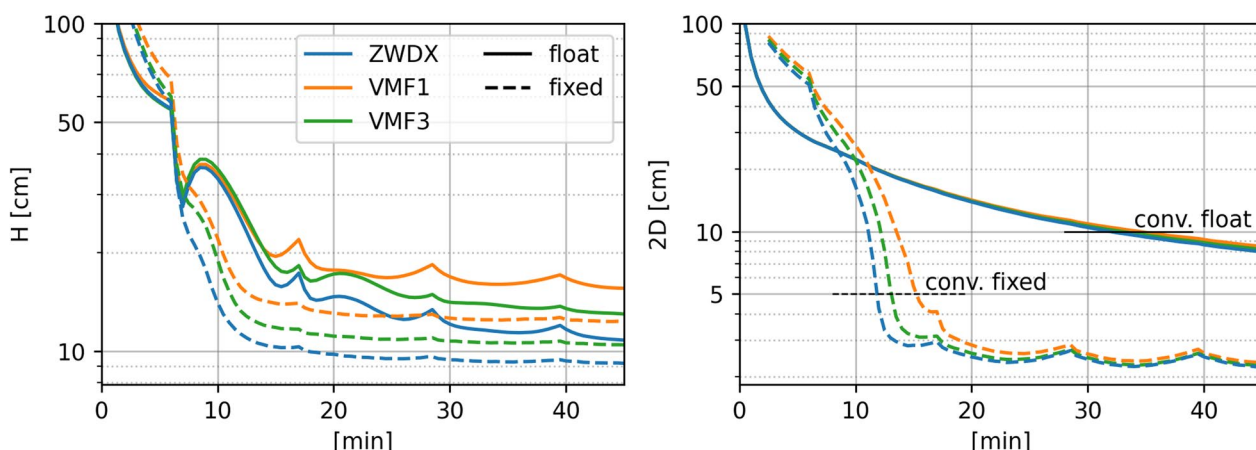
Page 11 of 16

Fig. 7 95 % quantile of the height (left) and 2D position (right) accuracy as a function of time. Results based on ZWDX, VMF1, and VMF3 are depicted in blue, orange, and green respectively. The float solution is depicted as solid lines while the fixed solution is depicted as dashed lines. The convergence criteria thresholds based on the 2D accuracy are annotated in the right plot
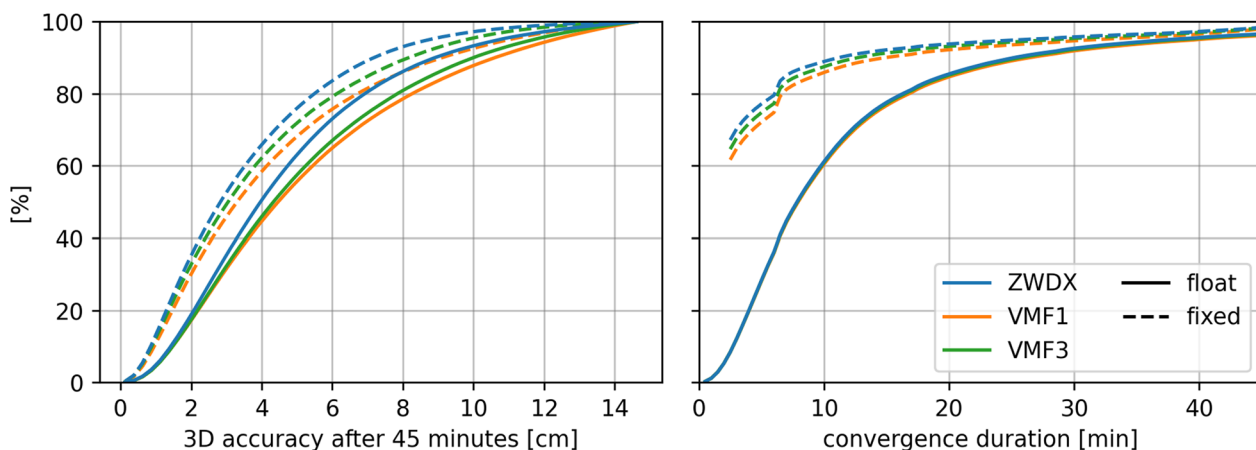

Fig. 8 Empirical cumulative density function of 3D positioning errors after 45 min (left) and time to convergence (right). Colors denote different troposphere models and solid vs. dashed lines denote the float and fixed solutions, respectively

independently and indirectly evaluate how well ZWDX estimates support a practical downstream application. As a benchmark, we compare results achieved with ZWDX to those with two state-of-the-art models, VMF1 and VMF3. The float and fixed PPP coordinate estimates are compared with the daily IGS coordinate solutions, which serve as ground truth.

Figure 7 displays the position accuracy (95% quantile of the positioning errors over all convergence periods) as a function of time, for both the float and fixed solution. The left graph shows height errors and the right one shows the 2D position errors. In the float solution, the 2D accuracy is not affected by the choice of ZWD model, whereas for the height, ZWDX performs best, followed by VMF3.

The impact of the ZWD model on the fixed solution is more pronounced. The reason is that integer ambiguity fixing is based on the float ambiguities, partly absorbing imperfections of the troposphere model. Consequently, the contaminated float ambiguities compromise the fixing of integer ambiguities and, with it, the quality of the fixed coordinate solution. Again, VMF1 performs worst, while ZWDX reaches the best accuracy and the fastest convergence time. Furthermore, the height component is more sensitive to imperfections of the troposphere model than the 2D position due to stronger correlations.

The left graph in Fig. 8 shows the cumulative histogram of 3D positioning errors for the final estimates after 45 min, for both the float and fixed solutions. It is evident that ZWDX reaches high accuracies more
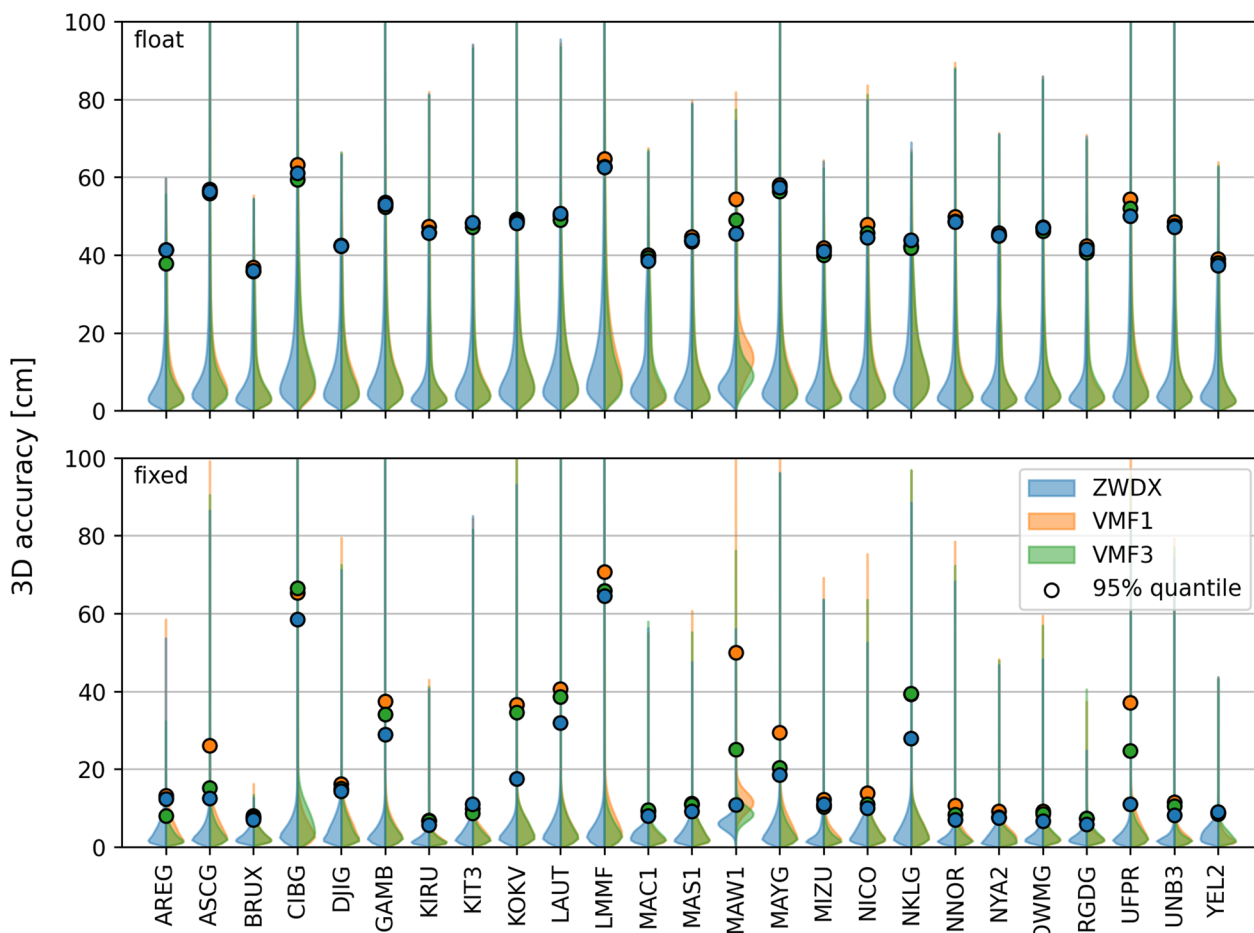
Fig. 9 3D position accuracy from the float solution (top) and fixed solution (bottom). Results based on ZWDX, VMF1, and VMF3 are depicted in blue, orange, and green respectively. The solid areas represent the accuracy distribution (aligned right for ZWDX and left for VMF1 and VMF3). The circles represent the 95 % quantiles

often than VMF3, which in turn outperforms VMF1. The right graph shows the associated cumulative histogram of convergence times. Convergence times for the float solution are unaffected by the choice of ZWD model, whereas the fixed solution converges fastest with ZWDX and slowest with VMF1. More detailed statistics that further support these observations are listed in Tables 3 and 4 in the appendix.

Figure 9 depicts the distribution of station-wise 3D accuracies for the float (top) and fixed (bottom) solutions. As explained above, the impact of different ZWD models is more pronounced for the fixed solution. While the differences are generally small, there is again a fairly consistent ranking, with ZWDX performing best and VMF1 performing worst. Interesting cases with relevant differences include stations MAW1 (Antarctica), UFPR (Brazil), and KOKV (Hawaii). At these stations, we can observe considerable differences in accuracy, highlighting once more the robustness

of ZWDX across different geographic and climatic regimes.

5 Conclusions and outlook

We have introduced ZWDX, a novel model capable of predicting ZWD values anywhere on Earth. Its novelty lies in a fully data-driven design. Rather than rely on hand-crafted relations derived from physical intuition, ZWDX derives its predictive skill from training on vast amounts of paired ERA5 reanalysis and NGL ZWD data, prioritizing predictive skill over low-dimensional, interpretable equations. The model has been evaluated on an independent test set of more than 200 million samples. ZWDX is generic and applicable across a range of tasks that require knowledge of ZWD, ranging from VLBI through PPP all the way to GNSS meteorology and climate analysis. Its stable performance when driven with HRES forecasts instead of ERA5 data also opens the door for real-time applications that necessitate (short-range)
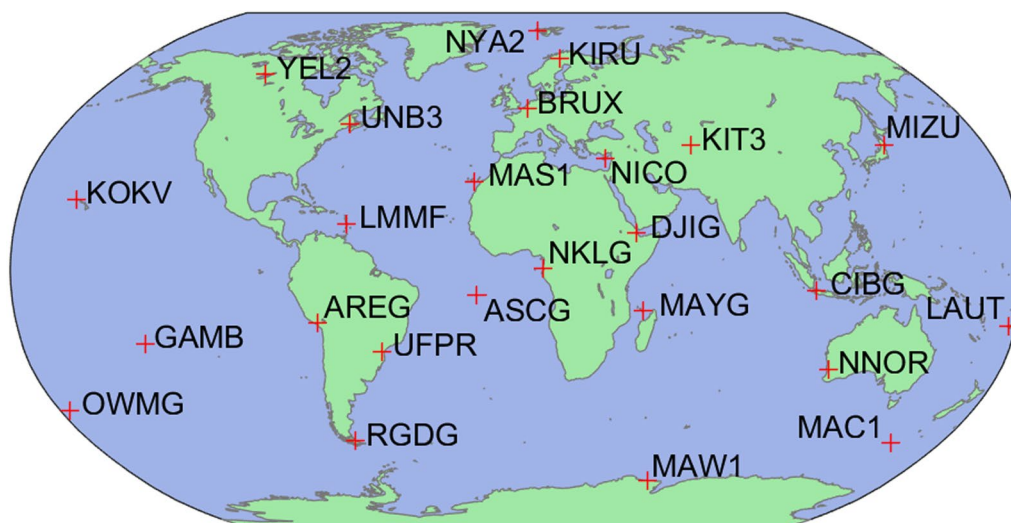
Crocetti *et al. Earth, Planets and Space* (2024) 76:163

Page 13 of 16

Fig. 10 Location of the 25 globally distributed IGS MGEX stations used in the PPP analyses

ZWD forecasting. A practical advantage of ZWDX is that it is simple to use and does not require the user to download any external data.

Specifically, ZWDX employs the XGBoost algorithm and has been trained on a large set of observations from 16,664 globally distributed GNSS stations, collected hourly over the period 2010–2021. ZWDX takes as input the geographical location, time of year, time of day, and specific humidity values at nine pressure levels. During training, specific humidity values from the ERA5 reanalysis are used as input. Due to its large and comprehensive training set of over $8.2 \cdot 10^8$ samples, distributed across the globe and spanning 12 years, the model is globally applicable and able to extrapolate outside of the training period. Consequently, ZWDX is also suitable for real-time ZWD forecasting by utilizing specific humidity values from the HRES forecasts predicted with meteorological models.

The model was evaluated at 2500 GNSS stations not included in the training set, and using observations from the year 2022, i.e., outside of the observation period used for training. With ERA5 reanalysis data as input, it achieves a WRMSE of 10.8 mm. Since ERA5 data is only available with a latency of 5 days, adjustments must be made for real-time or forecasting applications. While it would, in principle, be possible to train a model that predicts ZWD values solely based on past ERA5 data, the data gap of several days would lead to high uncertainties. We therefore prefer to make predictions based on meteorological forecasts (in our case, HRES), even if these are inherently less reliable than reanalysis data. We have demonstrated that ZWDX performs well in such a real-time scenario, i.e., for short forecasting horizons

HRES can serve as a substitute for ERA5. For nowcasting (horizon 0 h), the results match those with reanalysis data, with a WRMSE of 10.1 mm. For lead times of up to 12 h—the most important range, given that HRES forecasts are updated every 6 h—the WRMSE remains below 10.8 mm. Even with lead times of 24 and 48 h the WRMSE remains below 17 mm. Also important is that the differences between ZWDX predictions based on either ERA5 or HRES barely exhibit spatial patterns and are normally distributed around zero. In other words, real-time predictions based on atmosphere forecasts do not have significant regional biases and are not expected to be systematically less accurate in any specific part of the world. Still, it may be interesting to also train a dedicated model for HRES data, and to compare it to our replacement scheme.

The robustness of the XGBoost algorithm, demonstrated in Crocetti et al. (2024b), makes the ZWDX model tolerant against moderate levels of input noise. Still, one limitation of the current model is that it lacks a mechanism to explicitly quantify the uncertainty of its output values. Moreover, also uncertainties in the meteorological input are not propagated through the model. Extending the model to handle variable and heteroscedastic uncertainties in its inputs (i.e., the specific humidity values) and to quantify the uncertainties of its outputs (i.e., the ZWD values) will be an important direction for future work.

To further investigate the impact of ZWDX on downstream GNSS processing, we employ it as a troposphere model for PPP and compare its performance to the state-of-the-art. The PPP analysis constitutes an indirect evaluation, but is independent of the training data

Crocetti *et al. Earth, Planets and Space*   (2024) 76:163

Page 14 of 16

Table 3 Statistics of the float solution for different tropospheric models

	ZWDX	VMF3	VMF1	Unit
Average convergence time	9.90	9.95	10.02	[min]
Percentage of no convergence	3.05	3.21	3.50	[%]
Median 3D position difference of all epochs	7.7	8.5	9.0	[cm]
Average 2D position difference after 45.0 min	2.8	2.9	3.0	[cm]
Average 3D position difference after 45.0 min	5.3	6.0	6.7	[cm]

Table 4 Statistics of the fixed solution for different tropospheric models

	ZWDX	VMF3	VMF1	Unit
Average time to correct fix	4.73	5.04	5.40	[min]
Percentage of no correct fix	1.18	1.31	1.56	[%]
Median 3D position difference of all epochs	3.1	3.4	3.7	[cm]
Average 2D position difference after 45.0 min	1.1	1.1	1.2	[cm]
Average 3D position difference after 45.0 min	3.9	4.3	4.9	[cm]

(ERA5 specific humidities and NGL ZWDs). Data from 25 independent GNSS stations operated by the IGS were processed with the open-source software raPPPid using either ZWDX, VMF1, or VMF3 to model tropospheric delays. The GNSS data were processed in blocks of 45 min, resulting in over $2.7 \cdot 10^5$ individual convergence periods for the positioning task. For float coordinate solutions, the height component was determined most accurately when using ZWDX (whereas there were no noticeable differences in the 2D coordinates). As a consequence, the fixed solution reached higher 3D positioning accuracy with ZWDX than with the other tropospheric delay models and also converged faster.

Beyond GNSS positioning, ZWDX has potential for GNSS meteorology and global climate analysis. In a complementary study, we already calculated global ZWD trends and anomalies over time and could confirm a positive trend in the Northern Hemisphere and a negative trend in the Southern Hemisphere. The study also revealed that (time-lagged) ZWD anomalies are indeed strongly correlated with the El Niño Southern Oscillation (Crocetti et al. 2024a). We believe that ZWDX's ability to efficiently generate global ZWD

fields and time series may also be valuable for further research in atmosphere and Earth system science.

The ZWDX model, as well as its hourly ZWD predictions on a 0.25° grid, are publicly available at the Geodetic Prediction Center of ETH Zurich.[4] Additionally, we provide an API where users can query ZWDX to receive ZWD values for a given location and time.

Appendix A

See Fig. 10 and Tables 3, 4.

Declarations

Competing interests
The authors declare that they have no competing interests.

Author details
[1]Institute of Geodesy and Photogrammetry, ETH Zurich, Robert-Gnehm-Weg 15, 8093 Zurich, Switzerland. [2]Department of Geodesy and Geoinformation, TU Wien, Wiedner Hauptstraße 8-10, 1040 Vienna, Austria.

---

[4] https://gpc.ethz.ch/Troposphere/; last access: 10.11.2024.

Crocetti *et al. Earth, Planets and Space*   (2024) 76:163

Page 15 of 16

References

Aichinger-Rosenberger M, Brockmann E, Crocetti L et al (2022) Machine learning-based prediction of Alpine foehn events using GNSS troposphere products: first results for Altdorf, Switzerland. Atmos Meas Tech 15(19):5821–5839. https://doi.org/10.5194/amt-15-5821-2022

Benevides P, Catalao J, Nico G (2019) Neural network approach to forecast hourly intense rainfall using GNSS precipitable water vapor and meteorological sensors. Remote Sens. https://doi.org/10.3390/rs11080966

Bertiger W, Bar-Sever Y, Dorsey A et al (2020) GipsyX/RTGx, a new tool set for space geodetic operations and research. Adv Sp Res 66(3):469–489. https://doi.org/10.1016/j.asr.2020.04.015

Bevis M, Businger S, Herring TA et al (1992) GPS meteorology: Remote sensing of atmospheric water vapor using the global positioning system. J Geophys Res Atmos 97(D14):15787–15801. https://doi.org/10.1029/92JD01517

Bi K, Xie L, Zhang H et al (2023) Accurate medium-range global weather forecasting with 3D neural networks. Nature 619(7970):533–538. https://doi.org/10.1038/s41586-023-06185-3

Bi H, Huang L, Zhang H et al (2024) A deep learning-based model for tropospheric wet delay prediction based on multi-layer 1D convolution neural network. Adv Sp Res 73(10):5031–5042. https://doi.org/10.1016/j.asr.2024.02.039

Blewitt G, Hammond W, Kreemer C (2018) Harnessing the GPS data explosion for interdisciplinary science. Eos. https://doi.org/10.1029/2018eo104623

Böhm J (2013) Atmospheric effects in space geodesy. Springer, Berlin, Heidelberg. https://doi.org/10.1007/978-3-642-36932-2

Böhm J, Werl B, Schuh H (2006) Troposphere mapping functions for GPS and very long baseline interferometry from European Centre for Medium-Range Weather Forecasts operational analysis data. J Geophys Res Solid Earth. https://doi.org/10.1029/2005jb003629

Böhm J, Kouba J, Schuh H (2009) Forecast Vienna Mapping Functions 1 for real-time analysis of space geodetic observations. J Geod 83(5):397–401. https://doi.org/10.1007/s00190-008-0216-y

Böhm J, Möller G, Schindelegger M et al (2015) Development of an improved empirical model for slant delays in the troposphere (GPT2w). GPS Solut 19(3):433–441. https://doi.org/10.1007/s10291-014-0403-7

Bonafoni S, Biondi R, Brenot H et al (2019) Radio occultation and ground-based GNSS products for observing, understanding and predicting extreme events: a review. Atmos Res 230(104):624. https://doi.org/10.1016/j.atmosres.2019.104624

Chen J, Gao Y (2024) A machine learning-based tropospheric prediction approach for high-precision real-time GNSS positioning. Sensors. https://doi.org/10.3390/s24102957

Chen T, Guestrin C (2016) XGBoost: a scalable tree boosting system. In: Proceedings of the 22nd ACM SIGKDD International Conference on Knowledge Discovery and Data Mining. Association for Computing Machinery, New York, KDD '16, pp 785-794. https://doi.org/10.1145/2939672.2939785

Crocetti L, Schartner M, Schindler K, et al (2024a) Modelling the troposphere with global navigation satellite systems, meteorological data and machine learning. In: IGARSS 2024–2024 IEEE International Geoscience and Remote Sensing Symposium, pp 1689–1692. https://doi.org/10.1109/IGARSS53475.2024.10640441

Crocetti L, Schartner M, Zus F et al (2024b) Global, spatially explicit modelling of zenith wet delay with XGBoost. J Geod 98(4):23. https://doi.org/10.1007/s00190-024-01829-2

Ding J, Chen J (2020) Assessment of empirical troposphere model GPT3 based on NGL's global troposphere products. Sensors. https://doi.org/10.3390/s20133631

Ding J, Chen J, Tang W et al (2022) Spatial and temporal variability of global GNSS-derived precipitable water vapor (1994–2020) and climate implications. Remote Sens. https://doi.org/10.3390/rs14143493

Ding J, Chen J, Wang J et al (2023) Characteristic differences in tropospheric delay between Nevada Geodetic Laboratory products and NWM ray-tracing. GPS Solut 27(1):47. https://doi.org/10.1007/s10291-022-01385-2

Geng J (2022) Introduction. In: Geng J (ed) GNSS seismogeodesy. Elsevier, Amsterdam, pp 1–19. https://doi.org/10.1016/B978-0-12-816486-0.00007-7

Glaner MF (2022) Towards instantaneous PPP convergence using multiple GNSS signals. PhD Thesis, TU Wien. https://doi.org/10.34726/HSS.2022.73610

Glaner MF, Weber R (2023) An open-source software package for precise point positioning: raPPPid. GPS Solut 27(4):174. https://doi.org/10.1007/s10291-023-01488-4

Guerova G, Douša J, Dimitrova T et al (2022) GNSS storm nowcasting demonstrator for Bulgaria. Remote Sens. https://doi.org/10.3390/rs14153746

He L, Yao Y, Xu C et al (2024) A new global ZTD forecast model based on improved LSTM neural network. IEEE J Sel Top Appl Earth Obs Remote Sens. https://doi.org/10.1109/JSTARS.2024.3391821

Hersbach H, Bell B, Berrisford P et al (2020) The ERA5 global reanalysis. Q J R Meteorol Soc 146(730):1999–2049. https://doi.org/10.1002/qj.3803

Johnston G, Riddell A, Hausler G (2017) The international GNSS service. In: Teunissen PJ, Montenbruck O (eds) Handbook of global navigation satellite systems. Cham, Springer International, pp 967–982. https://doi.org/10.1007/978-3-319-42928-1_33

Kouba J, Lahaye F, Tétreault P (2017) Precise point positioning. Springer International Publishing, Cham, pp 723–751. https://doi.org/10.1007/978-3-319-42928-1_25

Lam R, Sanchez-Gonzalez A, Willson M et al (2023) Learning skillful medium-range global weather forecasting. Science 382(6677):1416–1421. https://doi.org/10.1126/science.adi2336

Landskron D, Böhm J (2018a) Refined discrete and empirical horizontal gradients in VLBI analysis. J Geod 92(12):1387–1399. https://doi.org/10.1007/s00190-018-1127-1

Landskron D, Böhm J (2018b) VMF3/GPT3: refined discrete and empirical troposphere mapping functions. J Geod 92(4):349–360. https://doi.org/10.1007/s00190-017-1066-2

Li H, Wang X, Wu S et al (2021a) An improved model for detecting heavy precipitation using GNSS-derived zenith total delay measurements. IEEE J Sel Top Appl Earth Obs Remote Sens 14:5392–5405. https://doi.org/10.1109/JSTARS.2021.3079699

Li S, Xu T, Jiang N et al (2021b) Regional zenith tropospheric delay modeling based on least squares support vector machine using GNSS and ERA5 data. Remote Sens. https://doi.org/10.3390/rs13051004

Li Q, Yuan L, Jiang Z (2023) Modeling tropospheric zenith wet delays in the Chinese mainland based on machine learning. GPS Solut 27(4):171. https://doi.org/10.1007/s10291-023-01507-4

Li Q, Böhm J, Yuan L et al (2024) Global zenith wet delay modeling with surface meteorological data and machine learning. GPS Solut 28(1):57. https://doi.org/10.1007/s10291-023-01595-2

Liu Y, Zhao Q, Li Z et al (2022) GNSS-derived PWV and meteorological data for short-term rainfall forecast based on support vector machine. Adv Sp Res 70(4):992–1003. https://doi.org/10.1016/j.asr.2022.05.057

Łoś M, Smolak K, Guerova G et al (2020) GNSS-based machine learning storm nowcasting. Remote Sens. https://doi.org/10.3390/rs12162536

Lu C, Zheng Y, Wu Z et al (2023) TropNet: a deep spatiotemporal neural network for tropospheric delay modeling and forecasting. J Geod 97(4):34. https://doi.org/10.1007/s00190-023-01722-4

Rasp S, Hoyer S, Merose A et al (2024) WeatherBench 2: a benchmark for the next generation of data-driven global weather models. J Adv Model Earth Syst 16(6):e2023MS004019. https://doi.org/10.1029/2023MS004019

Selbesoglu MO (2020) Prediction of tropospheric wet delay by an artificial neural network model based on meteorological and GNSS data. Eng Sci Technol Int J 23(5):967–972. https://doi.org/10.1016/j.jestch.2019.11.006

Siemuri A, Selvan K, Kuusniemi H et al (2022) A systematic review of machine learning techniques for GNSS use cases. IEEE Trans Aerosp Electron Syste 58(6):5043–5077. https://doi.org/10.1109/TAES.2022.3219366

Ware R, Exner M, Feng D et al (1996) GPS sounding of the atmosphere from low earth orbit: preliminary results. Bull Am Meteorol Soc 77(1):19–40

Xia P, Xia J, Ye S et al (2020) A new method for estimating tropospheric zenith wet-component delay of GNSS signals from surface meteorology data. Remote Sens. https://doi.org/10.3390/rs12213497

Yang F, Guo J, Zhang C et al (2021) A regional zenith tropospheric delay (ZTD) model based on GPT3 and ANN. Remote Sens. https://doi.org/10.3390/rs13050838

Yuan P, Blewitt G, Kreemer C et al (2023) An enhanced integrated water vapour dataset from more than 10 000 global ground-based GPS stations in 2020. Earth System Science Data 15(2):723–743. https://doi.org/10.5194/essd-15-723-2023

Ziv SZ, Reuveni Y (2022) Flash floods prediction using precipitable water vapor derived from GPS tropospheric path delays over the Eastern

Mediterranean. IEEE Trans Geosci Remote Sens 60:1–17. https://doi.org/10.1109/TGRS.2022.3201146

Zus F, Dick G, Dousa J et al (2015) Systematic errors of mapping functions which are based on the VMF1 concept. GPS Solut 19(2):277–286. https://doi.org/10.1007/s10291-014-0386-4

Publisher's Note

Springer Nature remains neutral with regard to jurisdictional claims in published maps and institutional affiliations.